



**HAL**  
open science

## Localisation of excitation in InGaN epilayers

Vyacheslav Kachkanov, Kevin Peter O'Donnell, Sergio Pereira, Robert Martin

► **To cite this version:**

Vyacheslav Kachkanov, Kevin Peter O'Donnell, Sergio Pereira, Robert Martin. Localisation of excitation in InGaN epilayers. *Philosophical Magazine*, 2007, 87 (13), pp.1999-2017. 10.1080/14786430701342164 . hal-00513828

**HAL Id: hal-00513828**

**<https://hal.science/hal-00513828>**

Submitted on 1 Sep 2010

**HAL** is a multi-disciplinary open access archive for the deposit and dissemination of scientific research documents, whether they are published or not. The documents may come from teaching and research institutions in France or abroad, or from public or private research centers.

L'archive ouverte pluridisciplinaire **HAL**, est destinée au dépôt et à la diffusion de documents scientifiques de niveau recherche, publiés ou non, émanant des établissements d'enseignement et de recherche français ou étrangers, des laboratoires publics ou privés.



**Localisation of excitation in InGaN epilayers**

Journal:	<i>Philosophical Magazine &amp; Philosophical Magazine Letters</i>
Manuscript ID:	TPHM-06-Jul-0236.R2
Journal Selection:	Philosophical Magazine
Date Submitted by the Author:	02-Mar-2007
Complete List of Authors:	Kachkanov, Vyacheslav; Strathclyde University, SUPA Physics O'Donnell, Kevin; Strathclyde University, SUPA Physics Pereira, Sergio; Universidade de Aveiro, Fisica Martin, Robert; Strathclyde University, SUPA Physics
Keywords:	luminescence, semiconductors
Keywords (user supplied):	



## Localisation of excitation in InGaN epilayers

V. Kachkanov<sup>1</sup>, K.P. O'Donnell<sup>1</sup>, S. Pereira<sup>2</sup> and R.W. Martin<sup>1</sup>

<sup>1</sup>*SUPA, Department of Physics, University of Strathclyde, Glasgow, Scotland, UK*

<sup>2</sup>*CICECO and Departamento de Fisica, Universidade de Aveiro, Aveiro, Portugal*

### ABSTRACT

Energy scalability of the excitation-emission spectra of InGaN epilayers, quantum wells and light emitting diodes provided indirect evidence for a fundamental common cause of the remarkable optical properties of this commercially important semiconductor alloy. Phase segregation on the nano-scale (accidental quantum dot formation) has generally been accepted as the mechanism of the spectral energy scaling (O'Donnell et al, PRL 82, 237 (1999)). Recently, however, the downsizing of the InN bandgap, from 2 to about 1 eV, has prompted a re-examination of the observations. Here, we present new structural evidence of InGaN nanostructure, obtained from a comparative analysis of Ga and In K-edge EXAFS (Extended X-ray Absorption Fine Structure) of a wide range of  $\text{In}_x\text{Ga}_{1-x}\text{N}$  epilayer samples. The mean In-Ga and Ga-In next-nearest-neighbour (NNN) separations are found to be unequal in length for InN-poor ( $0.1 < x < 0.4$ ) samples. The degree of inequality *increases* with *decreasing* InN fraction  $x$ , and therefore correlates with luminescence efficiency in this range of alloy composition. We propose that the breakdown of In/Ga randomness in InGaN alloys is associated with efficient excitation-emission in blue-green light emitting devices. Although non-randomicity may lead to a weak quasi-localisation of excitation, through the suppression of energy back-transfer, the issue of strong exciton localisation in InGaN is not directly addressed by these results.

## 1. INTRODUCTION

Localisation of excitons by phase segregation<sup>1</sup> is routinely invoked to explain the high efficiency of InGaN luminescent devices in the face of defect densities much larger than those encountered in other semiconductor materials. The most convincing evidence in support of a correlated spatial and energy localisation of excitons is the micro-spectroscopic observation of a characteristic “spotty” luminescence texture with a length scale of order 100 nm in PL and CL micrographs of InGaN epilayers<sup>2</sup>.

While electron-hole localisation is widely accepted as a key to enhanced luminescence efficiency in solids, the origin of the localisation mechanism in InGaN is a matter of continuing dispute. Self-formed or ‘accidental’ InN quantum dots<sup>3,4</sup> or In-rich (properly, InN-rich) InGaN clusters<sup>5,6</sup> may act as centres for exciton localisation. However, the discovery of the narrow band gap of InN, recently downsized from 2 to about 1 eV<sup>7</sup>, makes it less likely that pure InN quantum dots can be solely responsible for InGaN luminescence, since quantum confinement in these structures would have to be very strong to upshift the emission energy by ~2 eV from the InN band edge to the visible spectral region at which device efficiencies are maximised: pure InN dots with emission near 3 eV necessarily contain only a few In atoms. In experimental terms, the problem of identifying the nano-scale structure of such poorly defined lumophores (“quantum whats”) with particular spectral features is very challenging, while the calculation of the spectral signatures of exemplars may lie beyond present theoretical capabilities. Moreover, it is quite difficult to imagine how assemblies (menageries) of small lattice animals with narrow spectral signatures, similar to those identified in spatially resolved photoluminescence experiments<sup>8</sup>, can give rise to a seemingly continuous range of emission energies.

1  
2 Transmission Electron Microscopy<sup>5</sup> (TEM) and Energy Dispersive X-ray  
3  
4 (EDX) imaging of InGaN quantum wells<sup>6</sup> (QW) have claimed to reveal InN-rich  
5  
6 clusters, embedded in wells, as distinct contrast spots with a characteristic size of  
7  
8 about 3 nm. (Other contributors to this issue will no doubt provide further instances  
9  
10 of such observations.) However, both TEM and EDX techniques involve exposure of  
11  
12 samples to high-energy (~100 keV) electron bombardment, which may by itself  
13  
14 induce phase separation in alloys<sup>9,10</sup>. X-Ray Diffraction (XRD) is another  
15  
16 experimental technique that can provide information about phase segregation, if  
17  
18 carefully applied. Many authors have reported double (or some higher multiple)  
19  
20 XRD peaks in  $\theta$ - $2\theta$  scans, and doublet luminescence peaks in emission spectra, of  
21  
22 InGaN epilayers on GaN<sup>11,12</sup>. These observations were casually ascribed to InN  
23  
24 clustering<sup>13</sup>, but it has since been shown that the attribution of distinct diffraction  
25  
26 peaks to separated phases depends upon an incorrect application of Vegard's law  
27  
28 which does not take into account the strain state of samples<sup>14</sup>. The joint observation  
29  
30 of a luminescence doublet and a split XRD peak can often be better explained by the  
31  
32 co-existence of *two* InGaN layers with the *same* InN fraction but *different* states of  
33  
34 strain: one layer at the sample surface is relaxed while the other lies close to the GaN  
35  
36 substrate, almost coherent with it<sup>15</sup>. The so-called "S-shape" of the temperature  
37  
38 dependence of the emission peak of InGaN samples has also been described in terms  
39  
40 of thermal redistribution of excitons among centres with a range of localisation  
41  
42 energies<sup>16</sup>. In certain cases, however, an S-shaped dependence will arise naturally if  
43  
44 an unresolved luminescence doublet of the kind described above has components  
45  
46 with very different temperature dependences<sup>17</sup>.  
47  
48  
49  
50  
51  
52  
53  
54  
55  
56  
57  
58  
59  
60

1  
2  
3  
4  
5  
6  
7  
8  
9  
10  
11  
12  
13  
14  
15  
16  
17  
18  
19  
20  
21  
22  
23  
24  
25  
26  
27  
28  
29  
30  
31  
32  
33  
34  
35  
36  
37  
38  
39  
40  
41  
42  
43  
44  
45  
46  
47  
48  
49  
50  
51  
52  
53  
54  
55  
56  
57  
58  
59  
60

We conclude from the above brief summary that, despite nearly 10 years of effort, no uncontested evidence of a relation between InN-GaN phase segregation and enhanced luminescence efficiency of InGaN has been obtained in any laboratory. But phase segregation should lead to a characteristic non-randomness in the distribution of cations in a common-anion pseudobinary alloy, and we should exploit experimental techniques that can reveal this. Extended X-ray Absorption Fine Structure (EXAFS) analysis provides a unique structural tool for the acquisition of information about the atomic environment of specific elements in a solid, the so-called local structure<sup>18</sup>. EXAFS is a modulation of the absorption coefficient above a characteristic X-ray absorption edge of the “target” atomic species. It results from the scattering of ejected photoelectrons by atoms in the immediate neighbourhood and their subsequent interference with the outgoing photoelectron wave. EXAFS analysis reveals the chemical nature and coordination number of the surrounding atoms and their radial separation from the central absorber.

Although it provides information about atomic interactions on a sub-nanometre scale, EXAFS is not a microscopic technique. Microscopies (such as TEM) provide top-down analysis, limited by issues of magnification and resolution, whereas EXAFS offers a bottom-up approach. EXAFS tells us about chemical bonding, co-ordination numbers, bond lengths and so on, working from the nearest to the next nearest neighbours (NNN) and beyond, to build up a "picture" of the average environment of a chosen atomic species in a sample. It is limited by the fact that more distant neighbours interact more weakly with the ejected photoelectron and are therefore less visible. In other words, EXAFS provides statistical information about

1  
2 the first few moments of the spatial distribution of near neighbours to a targeted  
3  
4 atomic species, e.g. Ga or In, in a solid.  
5

6  
7 Consider, by way of a guiding example, a “non-random alloy” to be formed  
8  
9 artificially by gluing a sample of InN to an equal one of GaN. Although the InN  
10  
11 fraction of this (very odd) sample will be exactly 50%, EXAFS on the In sub-lattice  
12  
13 will reveal only In atoms in NNN positions, whereas Ga atoms would have all-Ga  
14  
15 NNN, according to EXAFS. The degree of phase segregation in such a sample would  
16  
17 be estimated as total. Obviously, many other distributions of cation locations could  
18  
19 provide the same statistical result within experimental error.  
20  
21  
22

23  
24 In this contribution we present the first direct measurement of the degree of  
25  
26 phase segregation in InGaN alloys from a detailed analysis that compares the In and  
27  
28 Ga local environments for the complete range of  $\text{In}_x\text{Ga}_{1-x}\text{N}$  alloys accessible to the  
29  
30 EXAFS technique (roughly  $0.1 < x < 0.9$ ). We then attempt to relate this statistical-  
31  
32 structural information to the well-known luminescence properties of InGaN alloy.  
33  
34  
35  
36

## 37 38 **2. SAMPLES AND EXPERIMENTAL DETAILS**

39  
40  $\text{In}_x\text{Ga}_{1-x}\text{N}$  samples were grown either by Molecular Beam Epitaxy (MBE) or by  
41  
42 Metal-Organic Chemical Vapour Deposition (MOCVD). MBE samples with “low”  
43  
44 InN contents ( $x < 0.40$ ), and all of the MOCVD samples ( $0.1 < x \leq 0.4$ ), included an  
45  
46 InGaN epilayer, some 200–500 nm thick, grown on a 1-2  $\mu\text{m}$  thick GaN buffer layer  
47  
48 on sapphire. InN-rich MBE samples ( $x \geq 0.60$ ) were grown directly on sapphire  
49  
50 substrates without any buffer layers. The In/Ga ratio of all layers was measured using  
51  
52 wavelength dispersive X-ray (WDX) analysis in a Cameca SX100 Electron Probe  
53  
54 Micro-Analyser (EPMA). The intensities of characteristic X-ray emissions from In  
55  
56  
57  
58  
59  
60

1  
2 and Ga in the samples were compared with those from InAs (or InP) and GaN  
3 standards<sup>19</sup>.  
4  
5

6 EXAFS spectra were measured on stations 7.1 and 16.5 of the UK Synchrotron  
7 Radiation Source (SRS) at Daresbury Laboratory. The local structure of In and Ga  
8 atoms in InGaN epilayers was probed by means of In K-edge (27928 eV, station  
9 16.5) and Ga K-edge (10370 eV, station 7.1) EXAFS measured in Fluorescence  
10 (FLY) and Total Electron Yield (TEY) modes. On station 7.1, a Si(111) double  
11 crystal monochromator with sagittally bent second crystal and a nine element  
12 monolithic Ge detector were used to measure EXAFS spectra. A Si(200) double  
13 crystal monochromator along with a 30-element solid state Ge detector were used to  
14 collect EXAFS data on station 16.5. EXAFS measurements in TEY mode were done  
15 in a chamber filled with helium. A Keithley 427 amplifier was used to detect current  
16 associated with X-ray absorption. TEY probes a thin layer (~5 nm) close to the  
17 sample surface and was chosen for the detection of Ga K-edge absorption in order to  
18 avoid any contribution to the InGaN EXAFS signal from Ga atoms located in the  
19 buffer. FLY and TEY In K-edge EXAFS was also measured to investigate the  
20 possibility of surface segregation. Interatomic distances obtained from the In K-edge  
21 EXAFS of InGaN measured in TEY and FLY modes were found to be identical  
22 within the measurement error: this preliminary result shows that there are no  
23 significant structural differences on a local scale between the bulk of samples and  
24 thin layers close to the surface. Therefore, in what follows, In local structure  
25 parameters obtained by In K-edge FLY EXAFS will be compared with Ga local  
26 structure parameters obtained by Ga K-edge TEY EXAFS. The local structure  
27  
28  
29  
30  
31  
32  
33  
34  
35  
36  
37  
38  
39  
40  
41  
42  
43  
44  
45  
46  
47  
48  
49  
50  
51  
52  
53  
54  
55  
56  
57  
58  
59  
60



parameters of MBE and MOCVD grown InGaN epilayers are shown Tables I and Tables II respectively.

The model of the local structure used to simulate In or Ga EXAFS was restricted to the two closest atomic coordination spheres that are of greatest interest. (This model is simpler than that used by Blant *et al.*<sup>20</sup> and more reliable, since the contribution to EXAFS from nitrogen atoms in the third coordination sphere is rather weak and hard to resolve.) The first coordination sphere always comprised 4 nitrogen atoms. The second coordination sphere was a mixture of In and Ga atoms, with the total number of atoms fixed at 12. The In-In, Ga-Ga, In-Ga and Ga-In distances were refined separately. The ratio of cationic species (In to Ga) in the second coordination sphere was also varied during the fitting procedure to best fit the experimental EXAFS. This ratio serves as a useful check of self-consistency with the independently measured In/Ga ratio obtained by EPMA. The fit quality was examined using of the fit index R, which is defined by the expression:

$$R = \sum_i \left[ \left( \frac{1}{\sigma_i} \right) \left| \text{experiment}(i) - \text{theory}(i) \right| \right] \times 100\%, \quad (1)$$

where  $\frac{1}{\sigma_i} = [k(i)]^2 / \left( \sum_i [k(i)]^2 \left| \text{experiment}(i) \right| \right)$ . The validity of extra parameters for each EXAFS simulation was checked using a *reduced*  $\chi^2$  method:

$$\text{reduced } \chi^2 = \frac{1}{(N_i - N_v)} \sum_i \left( \frac{X_{data}(k_i) - X_{model}(k_i)}{\varepsilon_i} \right)^2, \quad (2)$$

where  $\varepsilon_i$  is the uncertainty at each point (assumed to be the same at each point),  $X_{data}$  and  $X_{model}$  are the experimental and model values of the EXAFS at the same point,  $N_i$  is the number of independent points and  $N_v$  is the number of variables used in the fitting. Since in the *reduced*  $\chi^2$  test, the assumption is made that the uncertainty is

1  
2 the same at each point, the values of *reduced*  $\chi^2$  was used for comparison of  
3  
4 competing models only. The difference in the parameter values between the best-fit  
5  
6 value and the value for which the fit index was increased by 5% was used to estimate  
7  
8 the fitting error. The representative EXAFS spectra and their Fourier Transforms  
9  
10 along with simulated data are shown in Fig. 1.  
11  
12

13  
14 High resolution XRD characterisation was performed on selected samples  
15  
16 using a double-crystal diffractometer. The instrumental angular resolution is about 30  
17  
18 seconds of arc. A flat Ge (444) monochromator and horizontal divergence slits with  
19  
20 widths of 100  $\mu\text{m}$  and a height of 2 mm were used to select Cu  $K_{\alpha_1}$  radiation. A  
21  
22 position sensitive detector was placed at a variable distance from the sample in an  
23  
24 achromatic geometry.  
25  
26  
27  
28  
29  
30

### 31 **3. RESULTS AND DISCUSSION**

#### 32 **3.1. EXAFS analysis.**

33  
34 Mikkelsen and Boyce (MB hereafter) were first to apply EXAFS to local structural  
35  
36 studies of semiconductor solid solutions<sup>21</sup>. They discovered that the nearest  
37  
38 neighbour (NN) bond lengths in InGaAs, viz. In-As and Ga-As, are similar in  
39  
40 magnitude to those of the binary constituents InAs and GaAs respectively but that the  
41  
42 *weighted average* of In-As and Ga-As bond lengths in InGaAs follows Vegard's law.  
43  
44 The bimodal distribution of NN bonds and their weak dependence on composition is  
45  
46 probably a universal property of pseudobinary alloys<sup>22</sup>: it has also been observed in  
47  
48 GaAsP<sup>23</sup>, CdMnTe<sup>24</sup> and ZnMnSe<sup>25</sup>. Concerning the next-nearest neighbour (NNN)  
49  
50 separations, i.e. the cation–cation distances, MB noted that in the absence of  
51  
52 clustering, the In-Ga separation (obtained from In-edge EXAFS) and the Ga-In  
53  
54  
55  
56  
57  
58  
59  
60

1  
2 separation (obtained from Ga-edge EXAFS) agree with each other very closely  
3  
4 throughout the whole composition range of InGaAs alloys. These distances were also  
5  
6 found to be closely comparable to the lattice constant,  $a$ , of the alloys that were  
7  
8 obtained from X-ray Diffraction (XRD) measurements which exemplified Vegard's  
9  
10 law.  
11  
12

13  
14 The In-N and Ga-N bond lengths for InGaN alloys are plotted in Fig. 2(a) as a  
15  
16 function of InN fraction. As expected, the distances for all alloys are close to the  
17  
18 average NN bond lengths of InN (2.15 Å) and GaN (1.95 Å) respectively, and show  
19  
20 relatively little variation (<5% overall) with composition, whereas, as shown in Fig.  
21  
22 2(b), the weighted mean of the In-N and Ga-N NN bonds varies linearly between  
23  
24 those of the binary constituents, in accordance with Ref. 21. However, when  
25  
26 comparing MBE and MOCVD samples of similar InN fraction, we find that the In-N  
27  
28 and Ga-N bond lengths are systematically *longer* in the MOCVD samples. We shall  
29  
30 refer to the weighted mean of the In-N and Ga-N distances as the average cation-  
31  
32 anion distance. For InN-rich MBE samples, the average cation-anion distance  
33  
34 coincides with the cation-anion distance predicted by Vegard's law. However, for  
35  
36 MBE samples, with InN fractions below 40%, the average cation-anion distance is  
37  
38 significantly smaller than that predicted. For comparable InN-poor MOCVD  
39  
40 samples, the average cation-anion distance is somewhat closer to the Vegard's law  
41  
42 prediction. These incidental effects, due to strain, have no bearing on the matter of  
43  
44 phase segregation and will be discussed later.  
45  
46  
47  
48  
49  
50

51  
52 In all samples the numbers of In and Ga atoms detected by EXAFS in the  
53  
54 second coordination sphere were found to be in agreement with those for a random  
55  
56 alloy with the In/Ga composition ratio measured by WDX. This result precludes  
57  
58  
59  
60

1  
2 strong clustering of pure InN dots in InGaN alloys. The In-In and In-Ga distances,  
3  
4 obtained from *In K-edge* EXAFS, and the Ga-In and Ga-Ga distances, obtained from  
5  
6 *Ga K-edge* EXAFS, are compared in Fig. 3. In-Ga and Ga-In distances coincide for  
7  
8 InN-rich MBE samples ( $x \geq 60\%$ ), and also for a single MOCVD sample with 40%  
9  
10 InN. However, for MBE and MOCVD samples with less than 40% InN, the In-Ga  
11  
12 and Ga-In separations differ significantly: *the mean In-Ga distance is consistently*  
13  
14 *larger than the mean Ga-In distance.* This difference in the length of “mixed cation”  
15  
16 separations provides a clear indication of a non-random distribution of cations in the  
17  
18 sample. In short, this result indicates the existence of InN-rich regions in InN-poor  
19  
20 material.  
21  
22  
23  
24

25  
26 A gross deviation from randomness in the distribution of cations, leading to  
27  
28 different coordination numbers of next-nearest cation neighbours, would indicate the  
29  
30 existence of profound clustering or strong phase segregation; this has been found in  
31  
32 EXAFS studies of Rare-Earth doped nitrides<sup>26,27,28</sup>, at impurity concentrations as low  
33  
34 as a few atomic per cent. In contrast, such large deviations from the random  
35  
36 distribution of cations have not been observed for InGaN epilayer samples in this  
37  
38 work. However, EXAFS fits have rather large uncertainties for the coordination  
39  
40 number (typically ~15%). For a smaller degree of phase separation, an alloy could  
41  
42 not be distinguished from a random alloy in terms of coordination numbers. On the  
43  
44 other hand, the deficit of Ga atoms observed in the average In local structure and the  
45  
46 corresponding deficit of In atoms in the average Ga local structure clearly indicates  
47  
48 the presence of InN-rich regions (and complementary GaN-rich ones) in our InN-  
49  
50 poor samples. Thus, the difference in “mixed cation” distances, reported here,  
51  
52  
53  
54  
55  
56  
57  
58  
59  
60

1  
2 indicates a *weak* phase separation in the form of InN-rich and GaN-rich InGaN  
3  
4 regions, which occurs predominantly at rather low InN fractions,  $x < 0.4$ .  
5

6  
7 Fig. 4 summarises the NNN data related to the difference in “mixed cation”  
8  
9 distances on the In and Ga sub-lattices as a function of InN content. It shows clearly  
10  
11 that the difference in separations, i.e. the degree of non-randomness, *increases* with  
12  
13 *decreasing* InN fraction. The disparity is always higher for MBE than for MOCVD  
14  
15 samples with the same InN fraction. The largest measured difference of 0.09 Å,  
16  
17 corresponding to about 2.8% of the corresponding lattice constant, is observed for an  
18  
19 MBE sample with a global InN fraction of ~27%. The trend for all MOCVD samples  
20  
21 and for most MBE samples is clearly that of increasing disparity of the Ga and In  
22  
23 sublattices with decreasing InN fraction.  
24  
25  
26  
27

28  
29 Since EXAFS tells us nothing directly about the spatial distribution of different  
30  
31 phases, it is important to distinguish the effects of In aggregation from those of  
32  
33 random compositional disorder on the local scale: in the case of random  
34  
35 compositional disorder, the distribution of cations, of whichever kind, is still *random*  
36  
37 and the average local structures of In and Ga will be the same. However in the case  
38  
39 of In aggregation, there is a real *difference* in the In and Ga local structures since on  
40  
41 average more In atoms are located in InN-rich regions and more Ga atoms in GaN-  
42  
43 rich regions; this is completely and trivially true for the totally segregated sample  
44  
45 presented in the introduction. For real samples, the situation is also quite clear if we  
46  
47 understand the limitations of the EXAFS technique.  
48  
49  
50  
51  
52  
53  
54  
55  
56  
57  
58  
59  
60

3.2. Relation to optical properties and XRD.

1  
2 We now attempt to reconcile the local structure results described above with  
3  
4 what is already known about the optical properties of the examined samples<sup>29,30,31,32</sup>.  
5  
6 Firstly, luminescence spectroscopy showed that the peak emission energies of  
7  
8 comparable MBE and MOCVD samples were somewhat different: the peak emission  
9  
10 energies of MBE samples are always lower than those of MOCVD samples of similar  
11  
12 composition<sup>29</sup>. This fact suggests that a higher degree of indium aggregation in MBE  
13  
14 samples, compared to MOCVD samples of the same average composition, produces  
15  
16 higher local InN fractions in InN-poor regions, leading to lower emission energies.  
17  
18 This clearly links the local structure with the emission properties and solves one  
19  
20 mystery.  
21  
22  
23  
24

25  
26 Next, the Stokes' shift between absorption and emission is largest for samples  
27  
28 with an intermediate range of InN content<sup>31,33,34</sup>, indicating that the highest degree of  
29  
30 exciton localisation occurs for this most mixed composition. However, the results  
31  
32 presented in this letter show that the In and Ga local structure is the same for In-rich  
33  
34 MBE samples ( $x \geq 60\%$ ) and for MOCVD InGaN sample with 40% of InN. In these  
35  
36 cases, exciton localisation can result only from compositional disorder in a random  
37  
38 alloy: there is no phase segregation in the InN-rich samples. Random disorder cannot  
39  
40 be detected by EXAFS since EXAFS provides an averaged picture of the local  
41  
42 structure of a particular atom. Therefore, the results of In and Ga local structure  
43  
44 studies by means of EXAFS suggest that in InGaN alloys with InN fraction less than  
45  
46 40% InN, excitons are localised on InN-rich InGaN regions, whereas for InGaN  
47  
48 alloys with InN fractions of 40% and more, exciton localisation is likely to be due to  
49  
50 random compositional disorder only. The appearance of InN-rich regions with  
51  
52 *decreasing* InN fraction compares well with the concurrent increase of InGaN  
53  
54  
55  
56  
57  
58  
59  
60

emission efficiency<sup>35</sup> suggesting further that InN-rich InGaN regions act as efficient exciton localisation and/or emission centres.

Finally, the statistics of phase segregation depends upon both the size and the composition of InN-rich (and corresponding GaN-rich) regions; EXAFS averages local structure configurations and does not distinguish between the two contributions. If, however, the observed difference between the “mixed” cation distances were to equal the difference of 0.36 Å between the lattice constants of InN and GaN, this would indicate a complete phase separation of InGaN into InN and GaN, i.e., in this special case almost all of the In and Ga atoms would be found in InN and GaN phases respectively. (Equivalently, if the “mixed” cation distances were found to be equal in length, there would be no phase separation). In the singular case of a two-phase mixture of InN dots and InGaN alloy quantum boxes, a splitting of the metallic shell peak in the Fourier transform of In EXAFS was clearly observed<sup>36</sup>.

Consider a separation into only 2 components by way of illustration. The ratio of the difference in the “mixed” cation bonds to the difference in lattice constants of the binary constituents acts as a metric of the degree of phase segregation in a non-random alloy; it is equal to the fraction,  $F$ , of In atoms residing in In-rich regions:

$$F = \frac{d_{InGa} - d_{GaIn}}{a_{InN} - a_{GaN}}. \quad (3)$$

Considering only a two-component mixture, the following relations can be written for the average InN composition of an alloy,  $x_{average}$ :

$$x_{average} = x_{In-poor}(1-f) + x_{In-rich}f, \quad (4)$$

$$f = \frac{Fx^{In-poor}}{(1-F)x^{In-rich} + Fx^{In-poor}}, \quad (5)$$

1  
2 where  $x_{In-rich}$  is the InN content of InN-rich regions,  $x_{In-poor}$  is the InN content  
3  
4 averaged over the rest of the material, and  $f$  is the filling factor, i.e., the partial  
5  
6 volume of the material occupied by the InN-rich regions. Assuming, as an educated  
7  
8 guess, that the InN fraction of the InN-rich phase is 10% greater than the average  
9  
10 content ( $x_{average}$ ), for the sample with highest degree of phase separation ( $x = 27\%$ ) an  
11  
12 estimation using equations (3), (4) and (5) shows that In-rich regions (with  $x_{In-rich} \approx$   
13  
14 30%) occupy ~25% of the total volume of this sample.  
15  
16  
17

18  
19 In order to compare the short range order probed by EXAFS with long range  
20  
21 order, Reciprocal Space Maps (RSM) were measured by High Resolution XRD of  
22  
23 MBE samples with average InN contents of 14%, 27% and 35%, as shown in Fig. 5.  
24  
25 Analysis of the RSMs reveals that the InGaN epilayer with lowest InN content is  
26  
27 nearly pseudomorphic (i.e.  $a_{InGaN} = a_{GaN}$ ), whereas samples with higher InN content  
28  
29 are partially relaxed. For the sample with  $x=27\%$ , partial phase segregation is  
30  
31 inferred from the two InGaN-related diffraction spots (different  $c$ , but the same  $a$   
32  
33 lattice constant) which correspond to regions of different InN content. Recall that the  
34  
35 difference in “mixed” cation distances of In and Ga local structures obtained from  
36  
37 EXAFS analysis (i.e. the degree of phase separation) was highest for this sample.  
38  
39 This may suggest that partial phase separation for this sample reaches the (high)  
40  
41 degree necessary for its detection by XRD. Calculations based upon elasticity  
42  
43 theory<sup>37</sup> estimate the InN fraction of the InN-rich phase to be  $x=31\%$ , fortuitously  
44  
45 close to the assumed InN content used for illustrative purposes above.  
46  
47  
48  
49  
50  
51  
52  
53

54 3.3. Influence of strain on EXAFS and XRD measurements.  
55  
56  
57  
58  
59  
60



The NNN separations determine the lattice constant  $a$  of a semiconductor alloy. In a random ternary alloy  $A_xB_{1-x}C$  the lattice constant  $a$  is the *average* NNN distance. Since the weighted average of  $A-A$  and  $B-B$  distances is expected to be close to the length of “mixed” cation  $A-B$  and  $B-A$  bonds, which should be equal in a random alloy, the “mixed” cation bond length is in fact the lattice constant  $a$  of a random alloy, which depends on the alloy composition  $x$  according to Vegard’s law:

$$a(A_xB_{1-x}C)=r(A-B)=r(B-A)=xr(A-A)+(1-x)r(B-B). \quad (6)$$

In a partially phase-separated alloy the weighted average of “pure” cation-cation distances and that of “mixed” cation-cation distances are expected to be close to the lattice constant  $a$ :

$$a(In_xGa_{1-x}N)=xr(In-In)+(1-x)r(Ga-Ga)=xr(In-Ga)+(1-x)r(Ga-In). \quad (7)$$

In the case of dilute InGaN samples with InN fraction less than 15%, for which no In atoms could be fitted to EXAFS of the second coordination sphere, the weighted average of In-Ga and Ga-Ga distances is expected to be close to the lattice constant  $a$ :

$$a(In_xGa_{1-x}N)=xr(In-Ga)+(1-x)r(Ga-Ga) \quad (8)$$

The lattice constants  $a$  calculated from NNN distances by equations (6), (7) and (8) are shown in Fig. 6. In the case of samples with In-rich and Ga-rich regions the weighted average of “pure” cation-cation bonds or that of “mixed” cation-cation bonds (whichever had smaller fitting errors) was taken to approximate the  $a$  lattice

1  
2 constant. The  $a$  lattice constants obtained by XRD are shown in Fig. 6(a) for  
3  
4 comparison. The agreement between EXAFS and XRD is seen to be very good.  
5

6  
7 For MBE samples the behaviour of the  $a$  lattice constant obtained from NNN  
8  
9 distances mirrors that of the NN In-N and Ga-N bondlengths described previously.  
10  
11 Since Vegard's law does not take into account the strain state of epilayers, such  
12  
13 biaxial strain is likely to be the cause of the shrinkage of both NN and NNN  
14  
15 distances observed in our samples. The existence of biaxial compressive strain is  
16  
17 confirmed by XRD, as shown in Fig. 5. For MOCVD samples, NNN distances shrink  
18  
19 due to the strain when the InN fraction exceeds 24%. The strain does not, however,  
20  
21 affect NN bond lengths in these samples. We conclude that MBE samples with InN  
22  
23 fraction less than 40% and MOCVD samples with InN fraction less than 25% are  
24  
25 subjected to compressive strain which is higher in MBE samples than in MOCVD  
26  
27 ones of the same InN content, whereas the set of In-rich MBE samples is essentially  
28  
29 relaxed, due to the extremely large lattice mismatch: the critical thicknesses of InN-  
30  
31 rich alloys grown directly on sapphire are close to zero. The case of MBE samples  
32  
33 where both NN and NNN distances shrink suggests that compressive strain in the  
34  
35 epilayers, imposed by the GaN substrates, is accommodated through both angle and  
36  
37 length distortion of cation-anion bonds. NN bonds remain almost unaffected when  
38  
39 NNN distances shrink due to strain in MOCVD samples: it is easier to bend bonds  
40  
41 than to stretch them, in agreement with theoretical calculations<sup>38</sup>.  
42  
43  
44  
45  
46  
47  
48  
49  
50

#### 51 3.4. Excitation-emission efficiency and localisation on a non-random lattice.

52  
53 The concluding section of our discussion treats in a somewhat speculative manner  
54  
55 possible connections between weak localisation, as related to the weak phase  
56  
57  
58  
59  
60

1  
2 segregation reported above, and strong localisation, related to accidental QD  
3  
4 formation, in InGaN alloys.  
5

6  
7 The starting point of the discussion is the excitation-emission model that was  
8  
9 first put forward in References 3 and 4. We suppose that photonic or electronic  
10  
11 excitation interacts with *delocalised* excitons in the (weakly) phase-separated alloy  
12  
13 InGaN. Luminescence, as always, is related to exciton localisation: if an exciton  
14  
15 cannot delocalise within a characteristic lifetime, the consequence is a luminescence  
16  
17 event (emission of a photon). Crudely speaking, the delocalised exciton is an  
18  
19 excitation of the GaN-rich sublattice, while localised excitons favour the InN-rich  
20  
21 sublattice. Energy delocalisation after localisation may be called back-transfer of  
22  
23 excitation (from localised to delocalised states). This leads to a decrease in  
24  
25 luminescence output if the back-transferred excitation becomes shunted somehow  
26  
27 into a non-radiative branch.  
28  
29  
30  
31  
32

33 The correlation of energy with composition in an alloy leads to an intimate  
34  
35 connection between spatial and energy (and therefore momentum) localisation of  
36  
37 excitons. In order to assign a definite energy to an exciton, we suppose that it has a  
38  
39 finite extent and normalises the portion of lattice with which it interacts; essentially it  
40  
41 'samples' the In/Ga ratio within its volume (another bottom-up method). While it is  
42  
43 clear that delocalised excitons have in general rather higher energy than localised  
44  
45 ones, it is difficult to know exactly what this means physically. There is a world of  
46  
47 difference between a Wannier and a Frenkel exciton. The mean difference in energy  
48  
49 between the peak of the emission and the edge of the excitation spectrum is Stokes'  
50  
51 shift.  
52  
53  
54  
55  
56  
57  
58  
59  
60

1  
2 Luminescence efficiency measures the ratio of the photon emission rate to the  
3 total rate of annihilation of delocalised excitons, regarded as quanta of the excitation.  
4 For the efficiency to attain its maximum value of unity, (i) excitation must  
5 preferentially reach emitting centres (whatever their nature) rather than non-radiative  
6 traps and (ii) back-transfer of excitation from emitting centres to delocalised states  
7 must be eliminated.  
8  
9

10  
11 For the first point, we note that the migration of excitation through a lattice is  
12 enhanced by percolation. We speculate that the complementarity of the Ga and In  
13 sublattices enhances the delivery of excitation to lumophores when the InN fraction  
14 is lower than the percolation threshold. By the same token, excitons localised on  
15 InN-rich regions of the lattice will not readily delocalise. Although the movement of  
16 excitons through an energy-disordered environment cannot be described simply as  
17 hopping of classical particles between lattice points, it may be significant that the  
18 percolation threshold defined in this way for the diamond lattice is 0.43, which  
19 corresponds approximately to the InN fraction separating random from non-random  
20 InGaN alloys. (Of course this may also say something about the formation of the  
21 alloy itself during growth: it is notable that no MOCVD material with  $x > 0.4$  has been  
22 reported in the literature.) As for the second point, transfer of excitation, whether  
23 forwards or backwards in energy terms, depends strongly upon the distances  
24 involved, whether the mechanism is dipole-dipole ( $\sim r^{-6}$ ) or via tunnelling  
25 (exponential). In this context we note that the mean forward-transfer distance (Ga-In)  
26 is shorter than the back-transfer distance (In-Ga) in strongly luminescent alloys. In  
27 this way a small symmetry breaking can have profound consequences. Finally, we  
28 call attention to recent results, also not yet well understood, related to the  
29  
30  
31  
32  
33  
34  
35  
36  
37  
38  
39  
40  
41  
42  
43  
44  
45  
46  
47  
48  
49  
50  
51  
52  
53  
54  
55  
56  
57  
58  
59  
60

1  
2 ferromagnetism of GaN doped with Gd<sup>39</sup>: in this system too the effects of percolation  
3  
4 (of spins) appear to increase as the impurity becomes more dilute.  
5  
6  
7  
8

## 9 CONCLUSIONS

10  
11 In summary, a difference between In and Ga local structures was observed by  
12 EXAFS investigations of certain InGaN epilayers and attributed to weak phase  
13 segregation into InN-rich and GaN-rich regions. An estimate of the extent of these  
14 regions can be made, with the simplest set of assumptions, but EXAFS provides no  
15 information about the spatial distribution or size of InN-rich regions. Remarkably,  
16 the degree of the phase separation was found to *increase* with *decreasing* InN  
17 fraction  $x$  in  $\text{In}_x\text{Ga}_{1-x}\text{N}$ . This observation correlates with a concurrent increase of  
18 luminescence efficiency, suggesting that *slightly* InN-rich clusters are responsible for  
19 efficient exciton localisation and recombination in InGaN light-emitting devices.  
20  
21 However, the (possibly spontaneous) formation of InN-richer regions in InN-poorer  
22 material remains to be explained in a fundamental way on the basis of an improved  
23 understanding of the growth thermodynamics of InGaN alloy.  
24  
25  
26  
27  
28  
29  
30  
31  
32  
33  
34  
35  
36  
37  
38  
39

40 The authors are grateful to Dr JFW Mosselmans for leading the InGaN EXAFS  
41 programme at SRS Daresbury Laboratory, to Dr Benjamin Hourahine for useful  
42 discussions, and to Professor Yasushi Nanishi, Professor Enrique Calleja, Dr Ian M.  
43 Watson and Dr Wim van der Stricht for providing the samples used in this study. V.  
44 Kachkanov acknowledges financial support from the Overseas Research Students  
45 Award Scheme, Strathclyde University and Daresbury Laboratory.  
46  
47  
48  
49  
50  
51  
52  
53  
54  
55  
56  
57  
58  
59  
60

1. Ho, I.H. and Stringfellow, G.B. Solid phase immiscibility in GaInN. *Appl. Phys. Lett.* **69**, 2701-2703 (1996).
2. *Low-dimensional Nitride Semiconductors*, edited by Bernard Gil, 1st ed. (Oxford University Press, 2002).
3. O'Donnell, K.P., Martin, R.W., Middleton, P.G. Origin of Luminescence from InGaN Diodes. *Phys. Rev. Lett.* **82**, 237-240 (1999).
4. Martin, R.W. *et al.* Exciton localization and the Stokes' shift in InGaN epilayers. *Appl. Phys. Lett.* **74**, 263-265 (1999).
5. Chichibu, S. *et al.* Spontaneous emission of localized excitons in InGaN single and multiquantum well structures. *Appl. Phys. Lett.* **69**, 4188-4190 (1996).
6. Narukawa, T. *et al.* Role of self-formed InGaN quantum dots for exciton localization in the purple laser diode emitting at 420 nm. *Appl. Phys. Lett.* **70**, 981-983 (1997).
7. Davydov, V.Yu. *et al.* Band Gap of Hexagonal InN and InGaN Alloys. *Phys. Stat. Sol. (b)* **234**, 787-795 (2002).
8. Okamoto, K. *et al.*, Confocal microphotoluminescence of InGaN-based light-emitting diodes. *J. Appl. Phys.* **98**, 064503 (2005).
9. Smeeton, T.M. *et al.* Electron-beam-induced strain within InGaN quantum wells: False indium "cluster" detection in the transmission electron microscope. *Appl. Phys. Lett.* **83**, 5419-5421 (2003).

10. Li, T. *et al.*, Indium redistribution in an InGaN quantum well induced by electron-beam irradiation in a transmission electron microscope, *Appl. Phys. Lett.* **86**, 241911-1 – 241911-3 (2005).
11. Feng, S.-W. *et al.* Thermal annealing effects on an InGaN film with an average indium mole fraction of 0.31. *Appl. Phys. Lett.* **83**, 3906-3908 (2003).
12. Chang, H.J. *et al.* Direct evidence of nanocluster-induced luminescence in InGaN epilayers. *Appl. Phys. Lett.* **86**, 021911-1– 021911-3 (2005).
13. Srinivasan, S., *et al.* Low Stokes shift in thick and homogeneous InGaN epilayers, *Appl. Phys. Lett.* **80**, 550-552 (2002).
14. O'Donnell, K.P. *et al.*, Structural analysis of InGaN epilayers. *J. Phys. C* **13**, 6977-6991 (2001).
15. Pereira S. *et al.* Interpretation of double x-ray diffraction peaks from InGaN layers. *Appl. Phys. Lett.* **79**, 1432-1434 (2001); Pereira, S. *et al.* Structural and optical properties of InGaN/GaN layers close to the critical layer thickness. *Appl. Phys. Lett.* **81**, 1207-1209 (2002).
16. Cho, Y.-H. *et al.* "S-shaped" temperature-dependent emission shift and carrier dynamics in InGaN/GaN multiple quantum wells. *Appl. Phys. Lett.* **73**, 1370-1372 (1998).
17. S. Pereira and K.P. O'Donnell, unpublished.
18. Gurman, S.J. Interpretation of EXAFS Data. *J. Synchrotron Radiat.* **2**, 56-63 (1995).

- 1  
2  
3  
4 19. Martin, R.W. *et al.* Microcomposition and Luminescence of InGaN Emitters.  
5  
6 *Phys. Stat. Sol. (a)* **192**, 117-123 (2002).  
7  
8  
9 20. Blant, A.V. *et al.*, EXAFS studies of plasma-enhanced MBE grown Group III-  
10  
11 Nitrides. *Mater. Sci. Eng. B* **50**, 38-41 (1997).  
12  
13 21. Mikkelsen, J.C., Boyce, J.B. Extended x-ray-absorption fine-structure study of  
14  
15 Ga<sub>1-x</sub>In<sub>x</sub>As random solid solutions. *Phys. Rev. B* **28**, 7130-7140 (1983).  
16  
17 22. Martins, J. L. and Zunger, A. Bond lengths around isovalent impurities and in  
18  
19 semiconductor solid solutions. *Phys. Rev. B* **30**, 6217-6220 (1984).  
20  
21 23. Wu, Z. *et al.* Extended x-ray-absorption fine-structure study of GaAs<sub>x</sub>P<sub>1-x</sub>  
22  
23 semiconducting random solid solutions, *Phys. Rev. B* **48**, 8694-8700 (1993).  
24  
25 24. Balzarotti, A. *et al.* Local structure of ternary semiconducting random solid  
26  
27 solutions: Extended x-ray-absorption fine structure of Cd<sub>1-x</sub>Mn<sub>x</sub>Te. *Phys. Rev. B* **30**,  
28  
29 2295-2298 (1984).  
30  
31 25. Pong, W.-F. *et al.* Extended x-ray-absorption fine-structure studies of Zn<sub>1-x</sub>Mn<sub>x</sub>Se  
32  
33 alloy structure. *Phys. Rev. B* **41**, 8440-8448 (1990).  
34  
35 26. Katchkanov, V. *et al.* Extended X-ray absorption fine structure studies of thulium  
36  
37 doped GaN epilayers. *Superlattices Microstruct.* **36**, 729-736 (2004).  
38  
39 27. Katchkanov, V. *et al.* Extended X-ray Absorption Fine Structure Studies of GaN  
40  
41 Epilayers Doped *in situ* with Er and Eu During Molecular Beam Epitaxy. *Mat. Res.*  
42  
43 *Soc. Symp. Proc.* **798**, Y5.10.1 (2004)  
44  
45 28. Katchkanov, V. *et al.* Extended X-ray absorption fine structure studies of GaN  
46  
47 epilayers doped with Er. *Opt. Mater.* **28**, 785-789 (2006).  
48  
49  
50  
51  
52  
53  
54  
55  
56  
57  
58  
59  
60



- 1  
2  
3  
4  
5  
6  
7  
8  
9  
10  
11  
12  
13  
14  
15  
16  
17  
18  
19  
20  
21  
22  
23  
24  
25  
26  
27  
28  
29  
30  
31  
32  
33  
34  
35  
36  
37  
38  
39  
40  
41  
42  
43  
44  
45  
46  
47  
48  
49  
50  
51  
52  
53  
54  
55  
56  
57  
58  
59  
60
29. Fernandez-Torrente, I. *et al.* Anomalous composition dependence of optical energies of MBE-grown InGaN, *Mat. Res. Soc. Symp. Proc.* **798**, 673-676 (2003)
30. O'Donnell, K.P. *et al.* The composition dependence of the  $\text{In}_x\text{Ga}_{1-x}\text{N}$  bandgap. *J. Cryst. Growth* **269**, 100-105 (2004).
31. Martin, R.W. *et al.* The composition dependence of the optical properties of InN-rich InGaN grown by MBE. *Mat. Res. Soc. Symp. Proc.* **831**, E3.6 (2005).
32. Hernández, S. *et al.* Raman scattering study of the InGaN alloy across the whole composition range. *J. Appl. Phys.* **98**, 013511-1 – 013511-5 (2005).
33. Kurouchi, M. *et al.* Growth and properties of In-rich InGaN films grown on (0001) sapphire by RF-MBE. *Phys. Stat. Sol. (b)* **241**, 2843-2848 (2004).
34. Wu, J. *et al.* Universal bandgap bowing in group-III nitride alloys. *Solid State Commun.* **127**, 411-414 (2003).
35. Mukai, T. Recent progress in group-III nitride light-emitting diodes. *IEEE J. Sel. Top. Quantum. Electron.* **8**, 264-270 (2002).
36. O'Donnell, K.P. *et al.* In K-edge extended X-ray absorption fine structure of InGaN epilayers and quantum boxes. *Mater. Sci. Eng. B* **93**, 150-153 (2002).
37. Pereira, S. *et al.* Strain and composition distributions in wurtzite InGaN/GaN layers extracted from x-ray reciprocal space mapping. *Appl. Phys. Lett.* **80**, 3913-3915 (2002).
38. Kim, K., Lambrecht, W.R.L., Segall, B. Elastic constants and related properties of tetrahedrally bonded BN, AlN, GaN, and InN, *Phys. Rev. B* **53**, 16310-16326 (1996).

1  
2  
3  
4 39. Dhar, S *et al.* Gd-doped GaN: A very dilute ferromagnetic semiconductor with a  
5  
6 Curie temperature above 300 K. *Phys. Rev. B* **72**, 245203 (2005).  
7  
8  
9  
10  
11  
12  
13  
14  
15  
16  
17  
18  
19  
20  
21  
22  
23  
24  
25  
26  
27  
28  
29  
30  
31  
32  
33  
34  
35  
36  
37  
38  
39  
40  
41  
42  
43  
44  
45  
46  
47  
48  
49  
50  
51  
52  
53  
54  
55  
56  
57  
58  
59  
60

For Peer Review Only

1  
2 **Figure 1.**  $k^2$ -weighted In K-edge FLY EXAFS (a) and their Fourier Transform  
3  
4 Moduli (b) for MBE InGaN epilayers.  
5  
6  
7

8  
9 **Figure 2.** In-N and Ga-N bonds (a) and weighted average of In-N and Ga-N bonds  
10  
11 (b) as a function of InN fraction. Solid lines are linear fits to the data.  
12  
13

14  
15 **Figure 3.** Next-nearest neighbour distances as a function of InN fraction in MBE (a)  
16  
17 and MOCVD (b) samples. Solid lines are linear fits to the data.  
18  
19  
20

21  
22 **Figure 4.** Difference between In-Ga distance of In local structure and Ga-In distance  
23  
24 of Ga local structure for MBE and MOCVD samples.  
25  
26  
27

28  
29 **Figure 5.** Asymmetric reciprocal space maps of GaN and InGaN (10.5) reflections  
30  
31 for MBE-grown samples with InN fraction of 13.5% (a), 27.3% (b) and 34.9% (c).  
32  
33 The vertical full lines and the tilted dashed lines indicate coherent growth to the GaN  
34  
35 buffer and full relaxation, respectively.  
36  
37  
38

39  
40  
41 **Figure 6.** The dependence of the lattice constant  $a$ , calculated from In and Ga local  
42  
43 structure parameters, on InN fraction for MBE (a) and MOCVD (b) samples. Solid  
44  
45 lines are a linear fits to the data.  
46  
47  
48  
49  
50  
51  
52  
53  
54  
55  
56  
57  
58  
59  
60

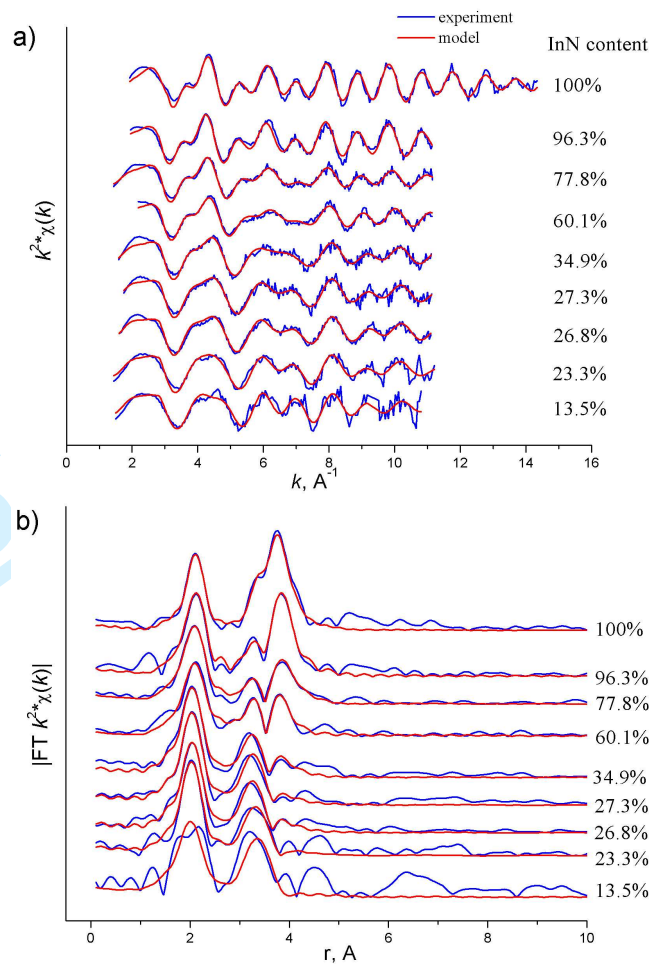


Figure 1.

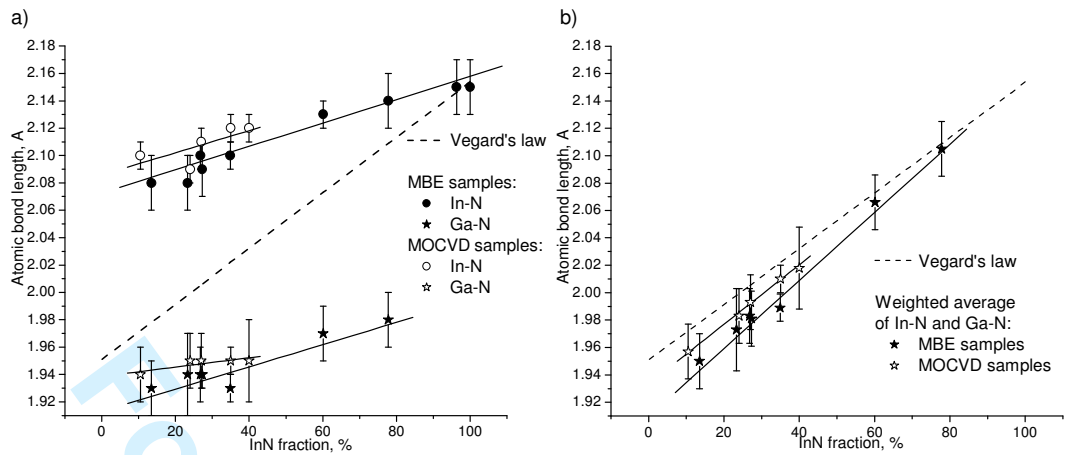
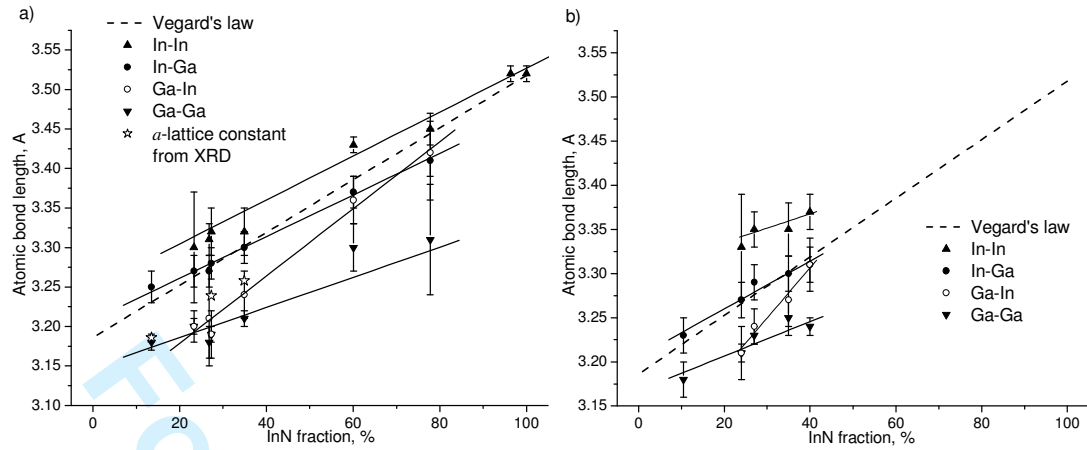


Figure 2.

**Figure 3.**

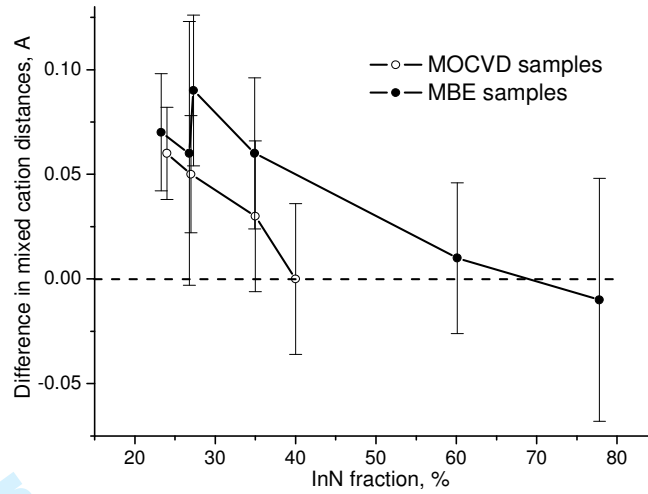


Figure 4.

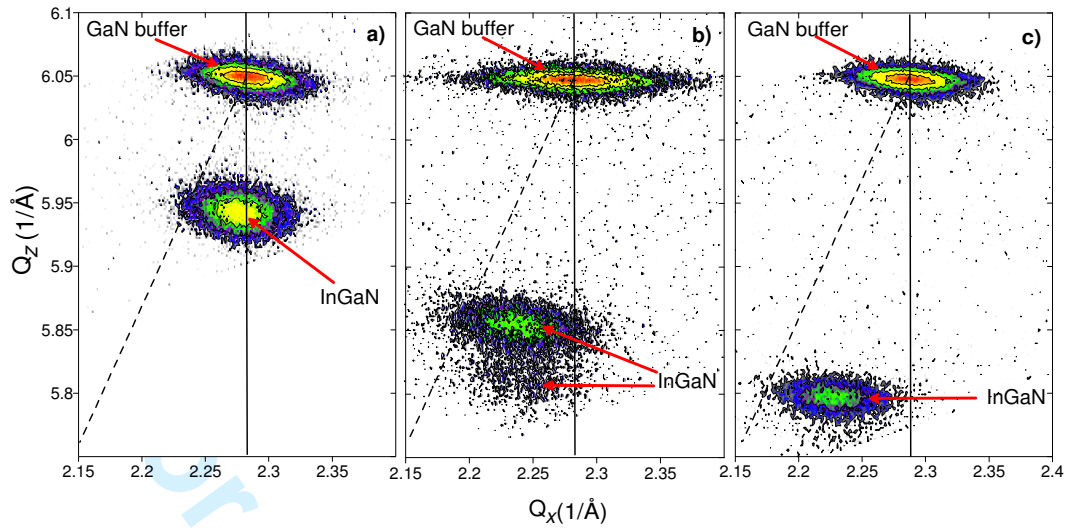


Figure 5.



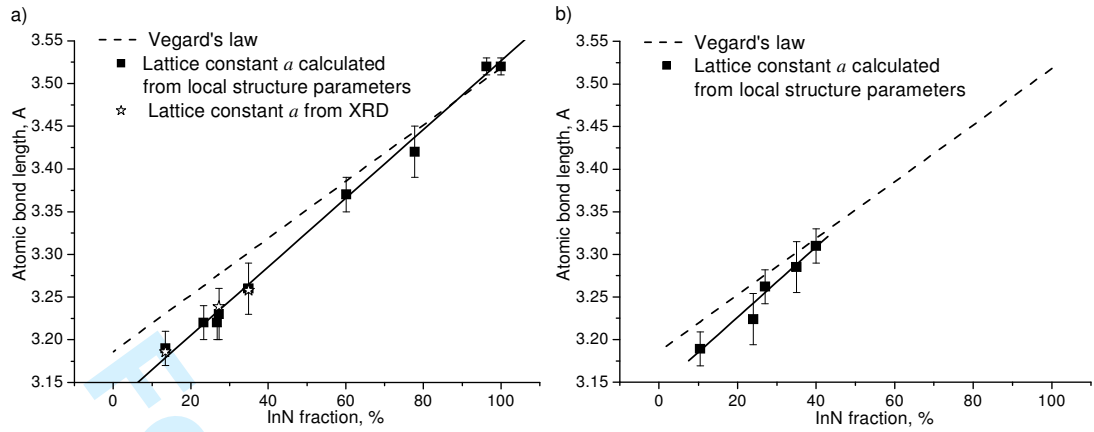


Figure 6.

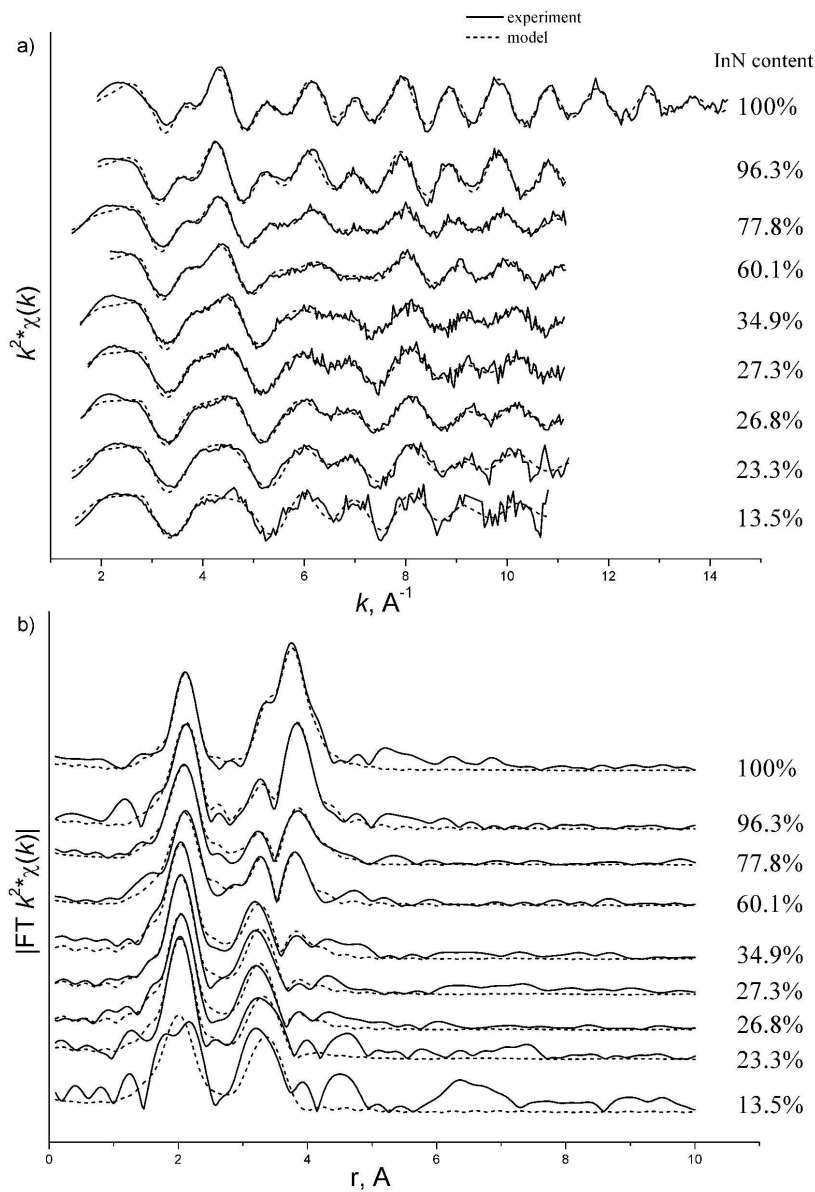
**Table I.** Local structure parameters for MBE grown InGaN epilayers.

InN content, %	Element and detection mode	Atom type	Number of atoms	Distance, Å	Debye-Waller factor, Å	$k$ range, Å <sup>-1</sup>	Fit index R
100	In K-edge FLY	N In	4 12	2.15±0.02 3.52±0.01	0.007 0.013	2-15	29.30
96.3	In K-edge FLY	N In	4 12	2.15±0.02 3.52±0.01	0.006 0.014	2-11	28.78
77.8	In K-edge FLY	N	4	2.14±0.02	0.010	1.5-11	30.69
		Ga	3.4±1.0	3.41±0.05	0.021		
		In	8.6±1.0	3.45±0.02	0.021		
77.8	In K-edge TEY	N	4	2.12±0.02	0.015	1.7-11	43.90
		Ga	4.0±1.8	3.39±0.06	0.023		
		In	8.0±1.8	3.44±0.02	0.023		
77.8	Ga K-edge TEY	N	4	1.98±0.02	0.014	2.5-13	35.94
		Ga	3.1±1.8	3.31±0.07	0.023		
		In	8.9±1.8	3.42±0.03	0.023		
60.1	In K-edge FLY	N	4	2.13±0.01	0.010	2-11	30.58
		Ga	4.3±0.9	3.37±0.02	0.017		
		In	7.7±0.9	3.43±0.01	0.017		
60.1	In K-edge TEY	N	4	2.13±0.01	0.006	2-11	29.78
		Ga	4.0±0.6	3.38±0.03	0.017		
		In	8.0±0.6	3.42±0.01	0.017		
60.1	Ga K-edge TEY	N	4	1.97±0.02	0.016	2.5-11	38.37
		Ga	6.0±1.3	3.30±0.03	0.020		
		In	6.0±1.3	3.36±0.03	0.020		
34.9	In K-edge FLY	N	4	2.10±0.01	0.006	1.7-11	34.20
		Ga	7.0±0.8	3.30±0.02	0.017		
		In	5.0±0.8	3.32±0.03	0.017		
34.9	Ga K-edge TEY	N	4	1.93±0.01	0.004	2.5-13	27.08
		Ga	9.4±0.7	3.21±0.01	0.015		
		In	2.6±0.7	3.24±0.03	0.015		
27.3	In K-edge FLY	N	4	2.09±0.02	0.005	1.8-11	33.61
		Ga	8.1±0.9	3.28±0.02	0.018		
		In	3.9±0.9	3.32±0.03	0.018		
27.3	In K-edge TEY	N	4	2.08±0.02	0.014	1.7-10.5	42.48
		Ga	9.2±1.8	3.26±0.02	0.019		
		In	2.8±1.8	3.33±0.09	0.019		
27.3	Ga K-edge TEY	N	4	1.94±0.01	0.006	2.5-13	31.39
		Ga	9.4±1.1	3.19±0.01	0.015		
		In	2.6±1.1	3.19±0.03	0.015		
26.8	In K-edge FLY	N	4	2.10±0.01	0.006	1.7-11	27.89
		Ga	8.0±0.9	3.27±0.02	0.017		
		In	4.0±0.9	3.31±0.02	0.017		
26.8	In K-edge TEY	N	4	2.08±0.02	0.009	2-11	41.59
		Ga	9.3±1.7	3.27±0.03	0.024		
		In	2.7±1.7	3.33±0.08	0.024		
26.8	Ga K-edge TEY	N	4	1.94±0.02	0.011	2.5-12	33.33
		Ga	9.8±1.0	3.18±0.02	0.013		
		In	2.2±1.0	3.21±0.06	0.013		
23.3	In K-edge FLY	N	4	2.08±0.02	0.005	1.5-11	36.92
		Ga	10.3±1.5	3.27±0.02	0.023		
		In	1.7±1.5	3.30±0.07	0.023		
23.3	In K-edge TEY	N	4	2.07±0.01	0.014	1.7-10	38.94
		Ga	10.6±1.2	3.25±0.02	0.022		
		In	1.4±1.2	3.30±0.30	0.022		
23.3	Ga K-edge TEY	N	4	1.94±0.03	0.003	2.5-13	37.25
		Ga	8.9±0.2	3.20±0.01	0.007		
		In	3.1±0.2	3.20±0.02	0.007		
13.5	In K-edge FLY	N	4	2.08±0.02	0.012	1.5-11	47.00
		Ga	12	3.25±0.02	0.024		
13.5	Ga K-edge TEY	N	4	1.93±0.02	0.008	2.5-13	34.42
		Ga	12	3.18±0.01	0.015		

**Table II.** Local structure parameters for InGaN samples grown by MOCVD.

InN content, %	Element and detection mode	Atom type	Number of atoms	Distance, Å	Debye-Waller factor, Å <sup>2</sup>	<i>k</i> range, Å <sup>-1</sup>	Fit index R
40	In K-edge FLY	N	4	2.12±0.01	0.007	1.5-11	25.12
		Ga	7.2±0.6	3.31±0.02	0.018		
		In	4.8±0.6	3.37±0.02	0.018		
	In K-edge TEY	N	4	2.11±0.01	0.006	2-12	40.20
		Ga	6.7±1.7	3.33±0.03	0.020		
		In	5.3±1.7	3.39±0.03	0.020		
Ga K-edge TEY	N	4	1.95±0.03	0.003	2.5-11	33.73	
	Ga	8.1±1.2	3.24±0.01	0.013			
	In	3.9±1.2	3.31±0.03	0.013			
35	In K-edge FLY	N	4	2.12±0.01	0.008	1.5-11	28.05
		Ga	8.0±0.8	3.30±0.02	0.019		
		In	4.0±0.8	3.35±0.03	0.019		
	In K-edge TEY	N	4	2.12±0.01	0.008	2-10.5	40.97
		Ga	7.1±2.0	3.31±0.04	0.022		
		In	4.9±2.0	3.35±0.03	0.022		
Ga K-edge TEY	N	4	1.95±0.01	0.008	2.5-11	24.73	
	Ga	8.7±0.8	3.25±0.02	0.015			
	In	3.3±0.8	3.27±0.03	0.015			
27	In K-edge FLY	N	4	2.11±0.01	0.008	1.5-11	27.98
		Ga	8.1±0.7	3.29±0.02	0.017		
		In	3.9±0.7	3.35±0.02	0.017		
	In K-edge TEY	N	4	2.09±0.02	0.010	2-10.5	36.77
		Ga	9.0±2.3	3.28±0.04	0.024		
		In	3.0±2.3	3.31±0.08	0.024		
Ga K-edge TEY	N	4	1.95±0.02	0.010	2.5-12	31	
	Ga	9.1±0.6	3.23±0.01	0.012			
	In	2.9±0.6	3.24±0.02	0.012			
24	In K-edge FLY	N	4	2.09±0.01	0.004	1.5-11	33.57
		Ga	8.6±1.3	3.27±0.02	0.021		
		In	3.4±1.3	3.33±0.06	0.021		
	In K-edge TEY	N	4	2.07±0.03	0.027	1.7-12	57.74
		Ga	9.4±2.2	3.27±0.03	0.021		
		In	2.6±2.2	3.31±0.06	0.007		
Ga K-edge TEY	N	4	1.95±0.02	0.010	2.5-12.5	28.89	
	Ga	9.8±0.7	3.21±0.01	0.012			
	In	2.2±0.7	3.21±0.03	0.012			
10.5	In K-edge FLY	N	4	2.10±0.01	0.005	1.5-11	31.35
		Ga	12	3.23±0.02	0.013		
	Ga K-edge TEY	N	4	1.94±0.02	0.004	2.5-13	37.31
		Ga	12	3.18±0.02	0.013		

1  
2  
3  
4  
5  
6  
7  
8  
9  
10  
11  
12  
13  
14  
15  
16  
17  
18  
19  
20  
21  
22  
23  
24  
25  
26  
27  
28  
29  
30  
31  
32  
33  
34  
35  
36  
37  
38  
39  
40  
41  
42  
43  
44  
45  
46  
47  
48  
49  
50  
51  
52  
53  
54  
55  
56  
57  
58  
59  
60



594x839mm (150 x 150 DPI)